Microwave Sensor with Hairpin Resonator-Based Line and Defected Ground Structure

Bruno Matias de Sousa, José Patrocínio da Silva and Valdemir Praxedes da Silva Neto

***Abstract*— This article proposes a Defected Ground Structure (DGS) based on the Thue-Morse sequence with a Hairpin-Based sensor optimized for S-band applications. The microwave sensor operates within a frequency range of 2.27 to 2.42 GHz and is constructed on a printed circuit board with a copper foil and FR-4 substrate, with a permittivity of 4.4 and a loss tangent of 0.02. The measured bandwidth was around 160 MHz and the transmission coefficient was -25 dB, with an average sensitivity measurement of 0.76% on the sensor. Despite a minor discrepancy observed in the return loss response value between the measured and simulated values, the proposed sensor is applicable to frequencies within the 2 to 4 GHz S-band.**

Keywords*— *Microwave sensor, Hairpin topology, Thue-Morse sequence.

I. INTRODUCTION

Nowadays, the incorporation of sensors using microwave technology has emerged as an efficient solution for applications in mobile satellite communications, especially in radar systems and communication networks that require operation at multiple frequencies [1]. The use of Defected Ground Structures (DGS) in these microwave sensors allows the development of hybrid circuits capable of providing high detection of permittivity, which are fundamental characteristics for meeting the performance requirements of modern communication systems [1].

The incorporation of DGS into hairpin resonator line designs has emerged as a promising strategy for improving the performance of these devices [3]-[6]. DGS involves the deliberate modification of the ground plane, resulting in benefits such as increased selectivity, reduced sensor size, and suppression of unwanted harmonics [7]. These improvements are particularly important in S-band, where stringent performance criteria are essential for applications such as radar and satellite communications [8].

Hairpin design have gained a notable presence in microwave engineering due to their compact size and efficient band-pass filtering capacity [9]-[10]. This microwave sensor configuration offers significant advantages in applications requiring high performance in a confined space, such as radar systems operating in the S-band (2-4 GHz) [11]. The use of microstrip hairpin topologies in switchable radar filter banks covering the S-band illustrates the efficiency and practicality of these filters in systems requiring fast switching between channels and high isolation of the filter elements [12].

Recent research into microwave with hairpin topology has focused on improving performance and addressing specific frequency bands. One study designed a hairpin filter for the 5G n77 band (3.3-3.4 GHz) using FR4 substrate, achieving an insertion loss of 5 dB at 3.35 GHz [13]. Another project incorporated radial stubs into hairpin resonators to suppress harmonics, demonstrating more than 32 dB of rejection up to 20 GHz for a 2 GHz center frequency filter. An ultra-wideband filter using high-temperature superconducting meander-line hairpin resonators with gradient linewidth achieved a bandwidth of 0.17% at 845.1 MHz with an insertion loss of 0.55 dB [14]. In addition, a microwave sensor based in hairpin resonator for detection Nitrogenous Fertilizers in Soil and Water is proposed, targeted the 6 GHz and high sensitivity [15].

In this study, a DGS structure based on the Thue-Morse sequence in the ground plane, combined with a square band, has been implemented in a microstrip hairpin resonator-based line for operation as a band-pass in the 2.27 to 2.42 GHz frequency range. This band is situated in the S-band, which is commonly used in satellite communication and radar navigation applications. To reduce manufacturing costs, the proposed sensor was developed on the FR-4 substrate. The design was first simulated in ANSYS HFSS software, and then a prototype was constructed to compare the results obtained in the simulations.

II. SENSOR STRUCTURE DESIGN

In this section, we describe important features of the device and its structural design. As defined in the literature, a filter is a device designed to pass certain frequencies while blocking or attenuating others, depending on its specific application. Several parameters are used in the filter to evaluate its performance, such as S-parameters, return loss, insertion loss, bandwidth, and others. These devices can be classified according to their frequency response, namely low-pass, high-pass, band-pass and band-reject.

A. Optimized Hairpin Resonator-based design

The topology used in this article was the microstrip band-pass filter based on the optimized Hairpin model. The traditional hairpin filter consists of an organized structure and its response is achieved by folding resonators into parallel coupled lines, forming half-wave resonators [16]. These resonators have a “U” shape.

However, the one used in this article contains an optimization in the structure of the resonators, an implementation of DGS in each resonator, as illustrated in Fig. 1 with references [17] and [18].

Bruno Matias de Sousa, Programa de Pós-Graduação em Engenharia Elétrica e Computação, Federal University of Rio Grande do Norte, Natal-RN, e-mail:bruno.matias.017@ufrn.edu.br; José Patrocínio da Silva, e-mail: jose.patrocinio@ufrn.br. Valdemir Praxedes da Silva Neto, Departamento de Engenharia de Comunicações, Federal University of Rio Grande do Norte, Natal-RN, e-mail: valdemir.praxedes@ufrn.br. This work was partially supported by Coordenação de Aperfeiçoamento de Pessoal de Nível Superior - Brasil (CAPES) – Finance Code 001.

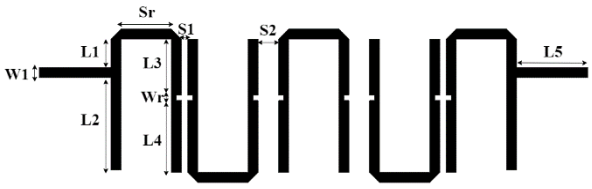

Fig. 1. Optimized Hairpin resonator.

The original design was adapted from [16], with adjustments made for the FR-4 substrate. To arrive at these dimensions, the authors first defined parameters that are obtained by manual calculation using existing formulas, such as width, length and the sliding factor.

1) Resonator width (W): It is obtained using the following calculations: For $W/h \leq 2$:

$$u = \frac{W}{h} = \frac{8 \cdot \exp(A)}{\exp(2A) - 2} \quad (1)$$

Where:

$$A = \frac{Z_c}{60}\sqrt{\frac{\epsilon_r + 1}{2}} + \frac{\epsilon_r - 1}{\epsilon_r + 1} \cdot (0{,}23) + \frac{0.11}{\epsilon_r} \quad (2)$$

Z_c is the characteristic impedance, and ϵ_r is the relative dielectric constant.

For $W/h \geq 2$, we have:

$$u = \frac{W}{h} = \frac{2}{\pi}[(B-1) - \ln(2B-1)] + \frac{\epsilon_r - 1}{2\epsilon_r}\left(\ln(B-1) + 0.39 - \frac{0.61}{\epsilon_r}\right) \quad (3)$$

$$B = \frac{60\pi^2}{Z_c\sqrt{\epsilon_r}} \quad (4)$$

$$W = u \times h \quad (5)$$

where W is the estimate of the width of the microstrip line that corresponds to the characteristic impedance Z_c, and h is the thickness of the dielectric, depending on the type of substrate.

2) Effective Dielectric Constant (ϵ_{eff}): The constant in a microstrip line can be determined using Equations (6) to (8).

$$\epsilon_{eff} = \frac{\epsilon_r + 1}{2} + \frac{\epsilon_r - 1}{2}\left(1 + \frac{10}{u}\right)^{-ab} \quad (6)$$

When,

$$a = 1 + \frac{1}{49}\ln\left[\frac{u^4 + \left(\frac{u}{52}\right)^2}{u^4 + 0.432}\right] + \frac{1}{18.7}\ln\left[1 + \left(\frac{u}{18.1}\right)\right] \quad (7)$$

$$b = 0.564\left(\frac{\epsilon_r - 0.9}{\epsilon_r + 3}\right)^{0.053} \quad (8)$$

3) Microwave line length (λ): It can be obtained using the Equations (9) e (10):

$$\lambda_{air} = \frac{c}{f} \quad (9)$$

$$\lambda_{microstrip} = \frac{\lambda_{air}}{\sqrt{\epsilon_{eff}}} \quad (10)$$

4) Resonator length: This is the size of the line used in the hairpin filter, which can be obtained by:

$$L = \frac{(90° - \theta°)}{360°} \times \lambda_{microstrip} \quad (11)$$

5) Dimension of the DGS implemented in the resonator: To obtain this value, Equation (12):

$$W_r = \frac{W1}{2} \quad (12)$$

B. Implementation of the DGS at Ground Level

Using the same dimensions as the reference work, but using the FR-4 substrate. The dimensions of the substrate and the thickness of the conductor are shown in Table I.

TABELA I. PROPOSED DIMENSIONS OF HAIRPIN RESONATOR LINE.

Parameter	h_{cond}	h_{sub}	*W1*	*Wr*	*Sr*	*S1*	*S2*	*L1*
Value (mm)	0.03	1.57	1.00	0.50	4.90	0.60	2.00	2.77
Parameter	*L2*	*L3*	*L4*	*L5*	*L*	*W*	L_{tm}	W_{tm}
Value (mm)	9.00	5.50	7.00	7.00	17.60	53.70	14.5	52.00

In this table, h_{cond} and h_{sub} represent the thickness of the conductor and substrate respectively, and L and W the dimensions of the substrate.

In order to improve the performance of the sensor, this work has implemented a DGS structure in the ground plane, adopting a configuration based on the Thue-Morse model. This choice was motivated by the growing search for new configurations capable of improving the efficiency and performance of this type of device. Thue-Morse is the infinite numerical sequence of zeros and ones. In the filter, this sequence is represented in the lower view by a square with a DGS structure. A one indicates the presence of a defect, while a zero indicates the absence of a defect. In the top view, the resonators are highlighted, allowing us to see the filter configuration as a whole, as shown in Fig. 2(a) and Fig. 2(b). The law of formation of Thue-Morse sequestration is given by:

$$t_n = s_2(n)(mod\ 2) \quad (13)$$

Where s_2 represents the binary sum, for $n = 0{,}1{,}2, \ldots$, where the first terms of the sequence are $0, 1, 1, 0, 1, 0, 0, 1, 1, 0, 0, 1$.

The DGS structure was proposed to see the effect on the behavior of the bandwidth increase for this particular case of a hairpin resonator-based line and to improve the sensor in this case.

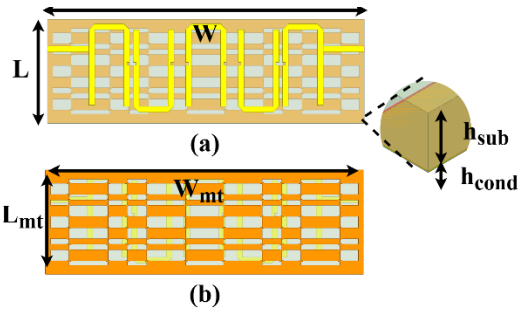

Fig. 2. Proposed microwave sensor with Hairpin resonator line at the top and DGS-based Thue-Morse sequence at the bottom. (a) Top view. (b) Bottom view.

III. RESULTS AND DISCUSSIONS

A. Simulated Results

The results of the simulation were used to develop the microwave sensor model in ANSYS-HFSS. This model was then simulated to obtain the values of the optimized topology. The values were obtained without the DGS structure and with the DGS structure of the Thue-Morse sequence. The results are shown in Fig. 3 below.

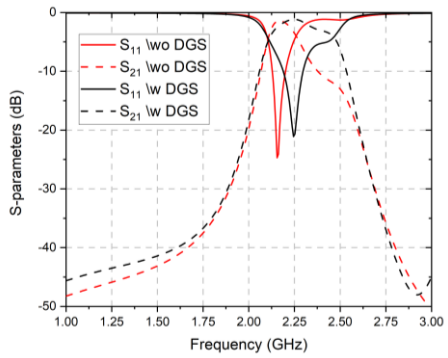

Fig. 3. Simulation results of the S-parameters, in dB, for the system without the DGS structure (in red) and with the DGS structure (in black) of the Thue-Morse sequence.

A desired resonance frequency of 2.16 GHz can be noted, corresponding to the frequency within the S-band and a bandwidth of 120 MHz. An insertion loss value of ≥ -3 dB was also chosen because it's a practical balance between size, cost, performance, and acceptable loss. We can see a simulated insertion loss of 1.43 dB.

For the simulated case with the DGS structure of the Thue-Morse sequence, a resonance frequency of 2.32 GHz was obtained, still corresponding to the S-band, and a bandwidth of 290 MHz. The simulated insertion loss of the DGS structure was 1.12 dB. We can initially see a shift in the resonance frequency compared to the original optimized structure and an increase in the bandwidth by 141.67%.

Fig. 4 shows the resonance frequency (f_r) of the S_{11} response in dB for the proposed sensor with the variation of this frequency in relation to the real relative permittivity (ϵ_r) of the material under test (MUT). It is possible to see a reduction in the resonance frequency as the permittivity increases, caused by an increase in the capacitance of the resonant element. For example, there is a band shift of around 70 MHz when the relative permittivity is increased from 1 to 10 and a shift of around 120 MHz from 1 to 80.

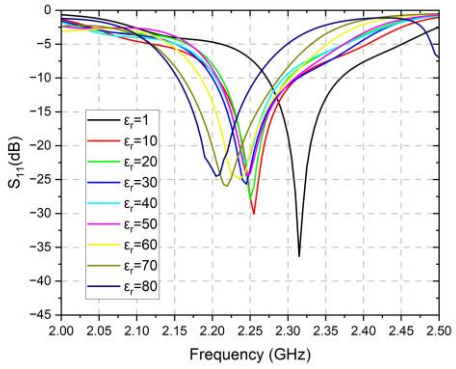

Fig. 4. Reflection coefficient, S_{11} (dB), for different MUT relative permittivity values.

The simulated variation of the relative permittivity of the MUT in relation to the resonance frequency shift of the sensor was studied. Data was collected to be analyzed through a curve fit and give us an approximate equation of the relationship of the real relative permittivity in relation to the simulated resonance frequency, as we can see in Fig. 5 and the curve equation (14) based on the 2nd-order polynomial technique found showed us a great approximation with $R^2 = 0.9991$ of the dataset points.

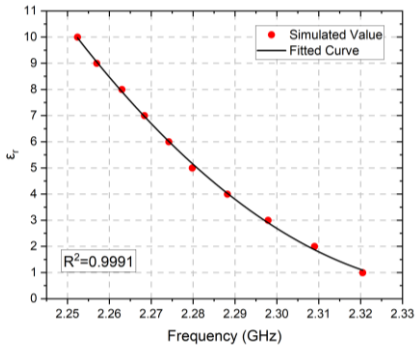

Fig. 5. Simulated value resonance frequency for different MUT (in red) relative permittivity values (1-10) and fitted curve associate (in black).

$$\epsilon_r(f_r) = 1103.38f_r^2 - 5176.00f_r + 6070.63 \quad (14)$$

B. *Setup and Experimental Results*

The proposed microwave sensor was manufactured using the acid corrosion technique under a 0.03 mm thick copper laminate with an FR-4 substrate with a dielectric constant of 4.4, a thickness of 1.57 mm and a loss tangent of 0.02. Two SMA connectors were used for the 50Ω ports. The total size of the board is 53 mm x 18 mm. Fig. 6(a) and Fig. 6(b) shows the manufactured prototype front and rear view of the proposed sensor with Thue-Morse sequence DGS structure.

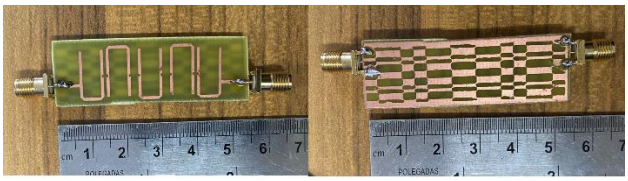

(a) (b)

Fig. 6. Prototyped microwave sensor. (a) Top view. (b) Bottom view.

Using a portable vector network analyzer model: LiteVNA (50 kHz - 6.3 GHz), the values of the factory filter were measured and compared to the results simulated in the electromagnetic simulation software. The parameters analyzed were its return loss, insertion loss and Smith's letter on the ports to see their match. The measurement setup in the laboratory is shown in Fig. 7 below.

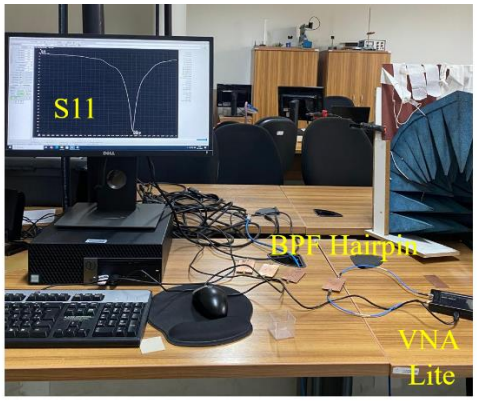

Fig. 7. Measurement setup.

Fig. 8 shows a comparison of the simulated and measured results for both sensors. The measured results show a resonance frequency of 2.17 GHz, a bandwidth of 220 MHz and an insertion loss ≥ -3 dB, with a value of 1.79 dB. It was possible

to see a deviation in the resonance frequency compared to the simulated response and a decrease in bandwidth of 24.14%. This result indicates a small loss for reasons inherent in the manufacturing process involved in the sensor.

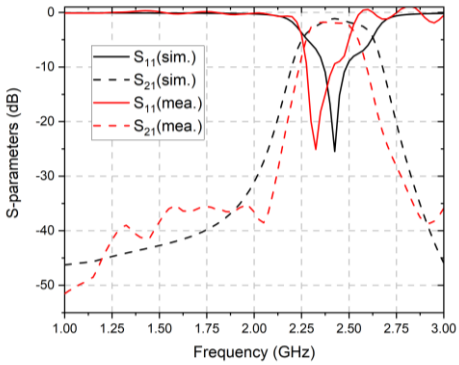

Fig. 8. Comparison of experimental (in red) and simulated (in black) measurements of the S-parameters of the proposed sensor with DGS Thue-Morse sequence.

To validate the efficiency of the proposed sensor, the sensor response of four different materials with different dielectric permittivity (RT Duroid 5880, FR4, RO3006 and RO3010) was measured, with actual relative permittivity ranging from 2.2 to 10.2. The measurement is shown in Fig. 9 of reflection coefficient for the different dielectric materials.

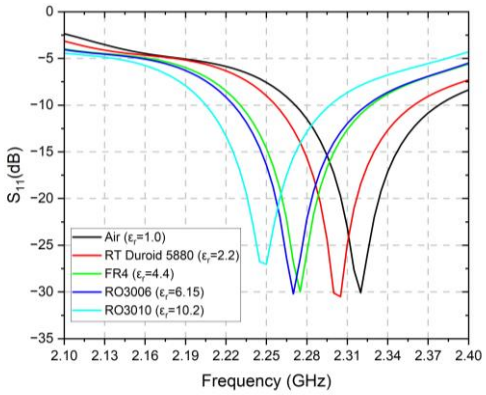

Fig. 9. Results S_{11} of the proposed sensor for different dielectric materials.

The measured variation of the relative permittivity of the MUT concerning the main dielectric materials used (Air, RT Duroid 5880, FR4, RO3006 and RO3010) in relation to the resonance frequency shift of the sensor was studied. Data was collected to be analyzed through a curve fit and give us an approximate equation of the relationship of the real relative permittivity in relation to the simulated resonance frequency, as we can see in Fig. 10 and the curve equation (15) based on the 3rd-order polynomial technique found give us a great approximation with $R^2 = 0.9905$ of the dataset points.

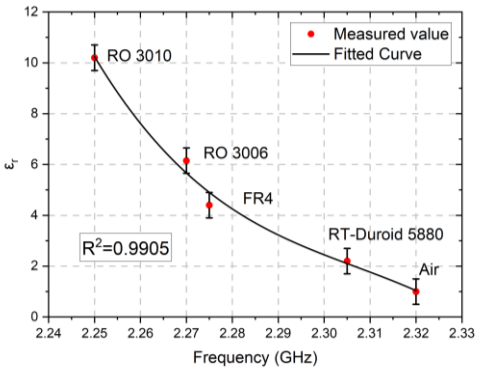

Fig. 10. Experimental results of resonance frequency for different MUT (in red) and fitted curve associate (in black).

$$\epsilon_r(f_r) = -24219.05f_r^3 + 167605.02f_r^2 - 386697.44f_r + 297449.23.63 \quad (15)$$

The following Table II presents a comparison of the real measured and ideal relative permittivity, alongside the percentage error of various MUTs. It is evident that the curve delineated in the equation (15) is in exact agreement with the ideal dielectric constant for the same samples. The minimum and maximum error detection achieved were 0.43% for RO3010 and 2.77% for FR4.

TABELA II. COMPARISON OF REAL MEASURED AND IDEAL RELATIVE PERMITTIVITY, SENSITIVITY AND PERCENTAGE ERROR DETECTION FOR THE PROPOSED SENSOR OF SEVERAL MUTS.

MUTs	**Ideal Dielectric Constant**	$\epsilon_r(measured)$	**Error (%)**	**Sensitivity (%)**
Air	1	1.021	2.04	-
RT Duroid 5880	2.2	2.172	1.27	4.8807
FR-4	4.4	4.522	2.77	1.3575
Roger 3006	6.15	6.053	1.58	0.8554
Roger 3010	10.2	10.244	0.43	0.3865

Table III shows a comparison between the proposed microwave sensor with previous works in literature applied to the S-band. It can be seen that our sensor performs better in terms of sensitivity than the others, as well as covering a higher real permittivity range.

TABELA III. PERFORMANCE COMPARISON WITH PREVIOUS WORKS.

Ref	**Frequency (GHz)**	ϵ_r **range**	S_{avg} (%)
[15]	6.00	1-25	0.70
[19]	2.17	1-10	0.70
This Work	2.32	1-80	0.76

IV. CONCLUSION

This work proposes the design of an optimized hairpin resonator-based line and DGS structure. The structure is both highly independent and compact; it is made up of a set of coupled microstrip lines on an FR-4 substrate. The ground plane of the structure is characterized by the presence of defects introduced almost periodically, inspired by the Thue-Morse sequence. Although the sensor is based on the conventional hairpin model, an optimization process using the DGS technique was applied to the ground plane.

The prototype demonstrated satisfactory performance for the intended application within the S-band frequency range. A comparison was conducted between the simulation results and the experimental findings, with a prototype constructed on a printed circuit board employing copper laminates and an FR-4 substrate. The experimental values for the minimum reflection coefficient, sensitivity, bandwidth, and resonance frequency obtained through measurement were -25 dB, 0.76%, 120 MHz, and 2.32 GHz, respectively. In conclusion, it is important to note that the model analyzed can be applied to S-band transmission and reception systems, such as radars and devices used in satellite communications.

ACKNOWLEDGEMENTS

This study was financed in part by the Coordenação de Aperfeiçoamento de Pessoal de Nível Superior - Brasil (CAPES) – Finance Code 001 and Programa de Pós-Graduação em Engenharia Elétrica e Computação (PPGEEC-UFRN)..

REFERENCES

[1] N. Krishna and K. Padmasine, “A review on microwave band pass filters: Materials and design optimization techniques for wireless communication systems,” Materials Science in Semiconductor Processing, vol. 154, pp. 107181–107205, 2023.

[2] D. F. Mamedes and J. Bornemann, “Band-pass hairpin filter using c-shaped dgs with wide-band rejection,” in 2022 IEEE International Symposium on Antennas and Propagation and USNC-URSI Radio Science Meeting (AP-S/URSI), pp. 277–278, 2022.

[3] T. Jiang, Q. An, and J. Wang, “Design of hairpin bandpass filter based on periodic grooves,” in 2021 6th International Conference on Integrated Circuits and Microsystems (ICICM), pp. 347–350, 2021.

[4] S. Achraou, A. Zakriti, B. B. S. Haddi, and M. E. Ouahabi, “Design of a miniaturized microstrip diplexer based on hairpin and short stub for 5g and wi-fi communications,” Progress In Electromagnetics Research Letters, vol. 112, pp. 67–75, 2023.

[5] G. M. Aristarkhov, I. N. Kirillov, O. V. Arinin, A. V. Markovskiy, and A. D. Doronina, “Multi-band bandpass microstrip filters based on two codirectional hairpin resonators,” in 2023 Systems of Signals Generating and Processing in the Field of on Board Communications, pp. 1–5, 2023.

[6] E. Shankar, K. V. P. Kumar, and V. K. Velidi, “A miniaturized dual narrow-band bandpass filter using a hairpin resonator and coupled lines,” in 2023 International Conference on Recent Advances in Electrical, Electronics, Ubiquitous Communication, and Computational Intelligence (RAEEUCCI), pp. 1–4, 2023.

[7] T. Singh, J. Chacko, N. Sebastian, R. Thoppilan, A. Kotrashetti, and S. Mande, “Design and optimization of microstrip hairpin-line bandpass filter using doe methodology,” in 2012 International Conference on Communication, Information Computing Technology (ICCICT), pp. 1–6, 2012.

[8] T. S. Alvi, M. H. Ahsan, M. Ali, F. Ramzan, K. A. Aljaloud, A. H. Alqahtani, R. Hussain, A. Alomainy, and M. Q. Mehmood, “A high-performance, low-cost, and integrated hairpin topology rf switched filter bank for radar applications,” Sensors (Basel), vol. 24, no. 2, pp. 1–16,2024.

[9] N. Ismail, S. M. Ulfah, I. Lindra, A. S. Awalluddin, I. Nuraida, and M. A. Ramdhani, “Microstrip hairpin bandpass filter for radar s-band with dumbbell-dgs,” in 2019 IEEE 5th International Conference on Wireless and Telematics (ICWT), pp. 1–4, 2019.

[10] Q. Abdullah, Aydoˆgdu, A. Salh, N. Farah, M. H. N. Talib, T. Sadeq, M. A. A. Al Mekhalfi, and A. Saif, “A compact size 5g hairpin bandpass filter with multilayer coupled line,” Computers, Materials Continua, vol. 69, p. 4025–4042, 2021.

[11] S. Rezaee and M. Memarian, “A compact microstrip combline filter for microwave s-band,” in 2021 29th Iranian Conference on Electrical Engineering (ICEE), pp. 891–894, 2021.

[12] V. B. Pusuluri, V. Mannam, V. A. S. Ponnapalli, and A. M. Prasad, “Narrowband hairpin bandpass filter for 4g lte applications,” in 2021 IEEE International IOT, Electronics and Mechatronics Conference (IEMTRONICS), pp. 1–5, 2021.

[13] A. S. S. Buñay, V. H. A. Moya, and A. J. V. Cevallos, “Diseño e implementación de un filtro microstrip pasa banda hairpin para la banda n77 de 5g,” Chone, Ciencia y Tecnología, vol. 2, pp. 1–16, 2024.

[14] X. Huang, X. Guan, B. Ren, and S. Wan, “A novel hts ultra-narrowband bandpass filter using hairpin meander-line resonator with gradient line-width,” IEEE Transactions on Applied Superconductivity, vol. 33, no. 2, pp. 1–5, 2023.

[15] A. Kundu, S. M. S. R. Hasan, S. Kapali, A. Helal, and K. Ali, “Hairpin resonator based microwave sensor for detection of nitrogenous fertilizers in soil and water,” IEEE Sensors Journal, vol. 24, no. 17, pp. 27436–27445, 2024.

[16] N. Ismail, T. S. Gunawan, S. Kartika, T. Praludi, and E. A. Z. Hamidi, “Design of microstrip hairpin bandpass filter for 2.9 ghz – 3.1 ghz sband radar with defected ground structure,” Malaysian Journal of Fundamental and Applied Science, vol. 14, no. 4, pp. 448–455, 2018.

[17] J. S. Hong and M. J. Lancaster, Advanced RF/Microwave Filters. New York: Wiley, 2001.

[18] N. Kinayman and M. Aksun, Modern Microwave Circuits. Norwood: Artech House, 2005.

[19] C.-F. Liu, M.-H. Wang, and L.-S. Jang, “Microfluidics-based hairpin resonator biosensor for biological cell detection,” Sensors and Actuators B: Chemical, vol. 263, pp. 129–136, 2018.